Synthesis of NiO/SnO_2 Nanowires for Energy Applications

H. Kaya*
Malatya Turgut Ozal University, Faculty of Engineering and Natural Sciences,
Department of Engineering Basic Sciences, Malatya 44210, Turkey

In this study, SnO_2 nanowire arrays with lengths in the micrometres range were successfully synthesised by using polyethylene glycol (PEG) at room temperature. Then Ni was coated onto the SnO_2 nanowires by chemical precipitation. These nanowires were heat-treated at 360, 450, 500, and 650 °C to form various phases. X-ray powder diffraction studies showed that the heat-treated sample at 500 °C has a tetragonal rutile SnO_2 phase. The Brunauer–Emmett–Teller surface area of the untreated $Sn(COO)_2$ nanowires was determined as 5.74 m^2/g. After Ni coating and heat treatment at 360, 450, 500, and 650 °C, the surface areas of the NiO/SnO_2 nanowires were measured to be 79.75, 33.38, 29.15, and 21.13 m^2/g, respectively.

DOI: 10.12693/APhysPolA.137.404

PACS/topics: SnO_2 nanowires, NiO-coated SnO_2 nanowires (NiO/SnO_2), supercapacitor, electrode, energy storage, PEG

1. Introduction

The need for energy increases proportionally with the development of technology. The energy we use at present is mainly provided by fossil fuels, which is highly damaging to the environment. Furthermore, studies have shown that fossil fuel use increases the formation of greenhouse gasses and thus, directly affects global warming. It is a fact, accepted by everyone, that eco-friendly energy sources are needed to minimise the consumption of fossil fuels. Recent studies have focused on the development of new products that may meet the energy requirements of devices in daily life, in addition to renewable energy sources. Supercapacitors stand out with their fast charge-discharge rate, excellent stability, long cycle life, and very high-power density in the energy storage field, compared to other energy storage devices [1–10]. Nanostructured materials are very impressive in the energy field as well as in other areas of technology due to their unique properties. Nanomaterials produced in different sizes and shapes have been used as an electrode material in supercapacitors. Besides the surface properties of the nanomaterial (nanowire, nanotube, nanoparticle, or nanoflake) which is used as an electrode, its type (such as carbon and derivatives, metal oxides, conductive polymers) is also another parameter that affects the performance of the supercapacitor. Metal oxide structures such as RuO_2, IrO_2, MnO_2, NiO, Co_2O_3, Co_3O_4, V_2O_5, and MoO_x [11–27] have been extensively studied in this area. Of these, ruthenium oxide is the most promising electrode material due to its high specific capacitance, high electrical conductivity, long cycle life, and good electrochemical reversibility. However, it is highly toxic and costly [27]. Efforts to develop new products in the field of energy have begun with the aim of reducing the high costs and the damage to nature. SnO_2, an n-type semiconductor with a bandwidth of 3.6 eV, is extremely cost-effective and eco-friendly [28, 29]. Only the SnO and SnO_2 phases are stable in the tin-oxide binary system that has various oxide phases [30]. Additionally, SnO_2 has applications in many areas of technology such as gas sensors, optoelectronic devices, magnetic recording, and magnetic resonance imaging systems [28–39]. The use of Sn, and Sn-based elements, in Na-ion, Li-ion batteries, and supercapacitors have recently been investigated [40]. It is suggested that the capacitance value of the pure SnO_2 structure is relatively low compared to some transition metal oxides. Ren et al. [41] obtained a specific capacitance value of 13.85 F/g at a scanning speed of 10 mV/s on an electrode made of SnO_2 microspheres. They coated the SnO_2 microspheres with carbon and increased the specific capacitance value to 43.3 F/g.

In this study, firstly, NiO was coated onto SnO_2 nanowires which were produced both cheaply and quickly. NiO was added to the structure to increase the relatively low specific capacitance of the SnO_2 nanowires.

2. Experimental

The steps followed in the production of nanowires containing Sn and Sn–Ni are outlined below. In the first step where SnO_2 nanowire production process is given, 150 ml of oxalic acid was completely dissolved in a mixture of 5 ml pure ethanol and 20 ml PEG (MW = 600). When the oxalic acid was completely dissolved, 35 mM $SnCl_2{\cdot}2H_2O$ was added to the solution. After the complete dissolution of the $SnCl_2{\cdot}2H_2O$ in solution, distilled water was added to the solution until a white precipitate formed and this was stirred for about 30 min. The solution was then washed twice, with distilled water and ethanol, and centrifuged at 9000 rpm for 15 min. The washed precipitate was dried in a vacuum oven at 60 °C for 24 h. The dried precipitate was heat-treated at 500 °C for 2 h at a rate of 1 °C/min.

*corresponding author; e-mail: harun.kaya@ozal.edu.tr

In the second step where Ni coating process to produced SnO_2 nanowires is given, Sn containing nanowires (about 0.1 g) were added to 50 ml of 50 mM $NiCl_2$ solution and stirred with a magnetic stirrer for one hour. Thereafter, 50 ml of 50 mM NH_4OH solution was added dropwise to this mixture at a rate of 1 ml/min and stirred with a magnetic stirrer at room temperature for 20 h. The NH_4OH dropping was performed with a "876 Dosimat Plus" automatic burette. After 20 h, the resulting solution was washed twice with distilled water and ethanol and centrifuged at 9000 rpm for 15 min. The washed precipitate was dried at 60 °C in a vacuum oven for 24 h. The nanowires containing Ni/Sn were subjected to heat treatment at 360, 450, 500, and 650 °C in an air environment using a linear temperature gradient tube furnace.

In the final step, where formation of electrode is given, 75% active material (SnO_2 or SnO_2/NiO NWs) and 15% acetylene black were ground and mixed in a Zr_2O_3 mortar for a certain time. Then 10% PVDF was added and this mixture was ground for one hour. A few drops of 1-methyl-2-pyrrolidinone were added into the homogeneous mixture and slurried. This slurry was dropped to spread over previously cleaned Ni foam. The resulting structure was dried in a vacuum oven at 60 °C for 24 h and then pressed under a pressure of 5 tons. Electrochemical measurements were performed using a 6 M KOH solution. Measurements were performed in an electrochemical cell consisting of a working electrode, platinum electrode, and an Ag/AgCl reference electrode. The cyclic voltammetry (CV), charge-discharge, and electrochemical impedance spectroscopy (EIS) measurements of the electrode were performed using a Gamry Reference 3000 potentiostat/galvanostat/ZRA instrument. The surface properties of the SnO_2, NiO/SnO_2 nanowires were investigated by using an FEI Nova Nano SEM 450 scanning electron microscope and thermogravimetric analyses (TGA) were carried out using a Shimadzu TGA-50 thermogravimetric analyser. The Brunauer–Emmett–Teller (BET) surface area, average pore diameter, and pore volume of the SnO_2, NiO/SnO_2 nanowires were determined using a Micromeritics Gemini VII 2390t instrument. X-ray diffraction (XRD) measurements were made using the Rigaku-RADB brand X-ray diffractometer.

3. Results and discussions

In Fig. 1 the TGA thermograms of the Sn nanowires and Ni/SnO_2 nanowires formed using PEG are shown. TGA measurements were carried out in an air environment at a rate of 10 °C/min. The TGA graph of the Sn nanowires produced using PEG, shows a single-stage uniform mass loss. The mass loss in the decomposition from room temperature to 420 °C is 29.6%. This mass loss is due to the evaporation of water on the surface of the material, decomposition of the oxalic acid and $SnCl_2$ as well as the PEG. It has been reported that PEG starts

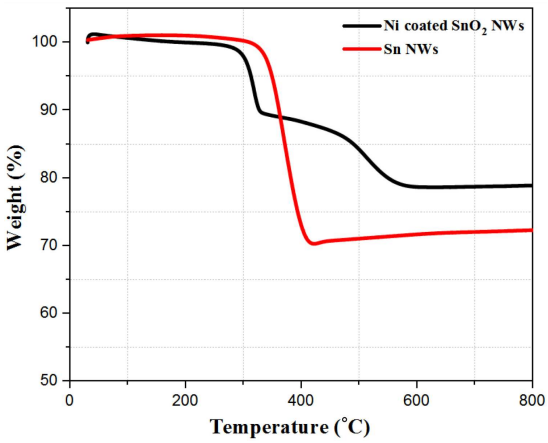

Fig. 1. TGA thermogram of Sn and Ni/SnO_2 nanowires.

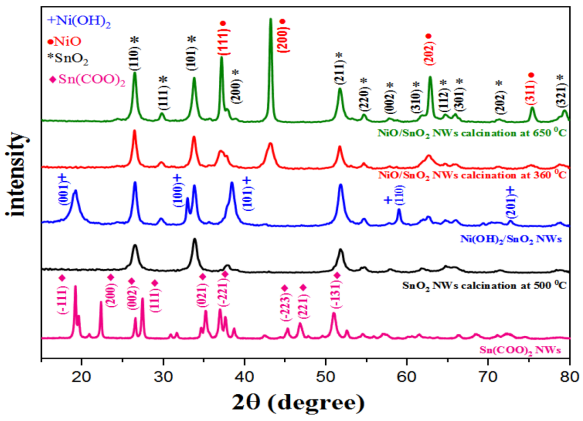

Fig. 2. XRD pattern of Sn-based and NiO/SnO_2 NWs at different calcination temperature.

to decompose at 340 °C and its degradation has ended at 415 °C with its mass loss being approximately 99% [42]. It can be said that the $Sn(COO)_2$ structure is completely converted to SnO_2 after 420 °C. This result was also supported by XRD measurements (Fig. 2). In the region up to 420 °C, it can be said that the polymer chains in PEG are thermally degraded and the mass loss of 29.6% belongs to Sn nanowires.

TGA analysis of the Ni-coated SnO_2 nanowires shows that mass loss occurs in three different temperature zones. In the first region (30–150 °C), 1.3% mass loss can be attributed to the removal of moisture in the structure and 10% mass loss in the 150 °C–330 °C range can be attributed to the continuous disposal of water and ethanol from the sample [43]. The mass loss of 12% in the 330 °C–600 °C temperature range suggested that dehydration of surface hydroxyl groups took place. In this region, the $Ni(OH)_2/SnO_2$ structure was completely transformed into NiO/SnO_2. Above 600 °C, no significant mass loss occurred and 77% of the material remained.

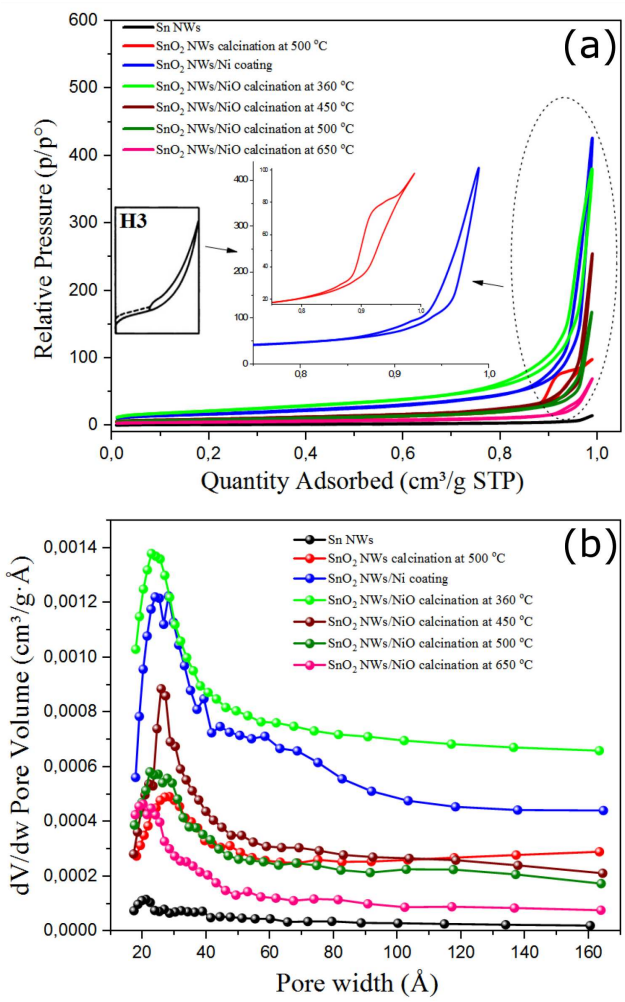

Fig. 3. (a) Nitrogen adsorption-desorption isotherm of SnO_2 and NiO/SnO_2 NWs at different calcination temperature. Inset shows the zoom of hysteresis area in nitrogen adsorption-desorption isotherm. (b) BJH pore size distribution.

Figure 3a shows N_2 adsorption-desorption curves of the SnO_2 and NiO/SnO_2 nanowires. While the BET surface area of the $Sn(COO)_2$ nanowires was 5.74 m^2/g, it was increased to 25.39 m^2/g for the SnO_2 nanostructures after heat treatment at 500 °C. The nickel plating of SnO_2 nanowires increased the BET surface area to 62.05 m^2/g. The BET surface areas of the heat-treated samples at 360, 450, 500, and 650 °C were 79.75, 33.38, 29.15, and 21.13 m^2/g, respectively. The adsorption isotherm, where micro (< 2 nm) and mesopores (2–50 nm) coexist (Fig. 3b) (according to the classification of the IUPAC), is known as type IV [44]. The nitrogen adsorption-desorption curves (Fig. 3a) are in good agreement with type IV isotherm, which exhibits a similar hysteresis H3 [44] curve seen in the pores formed by plane-like particles. XRD graphs of the materials containing Sn and Ni–Sn nanowires are given in Fig. 3.

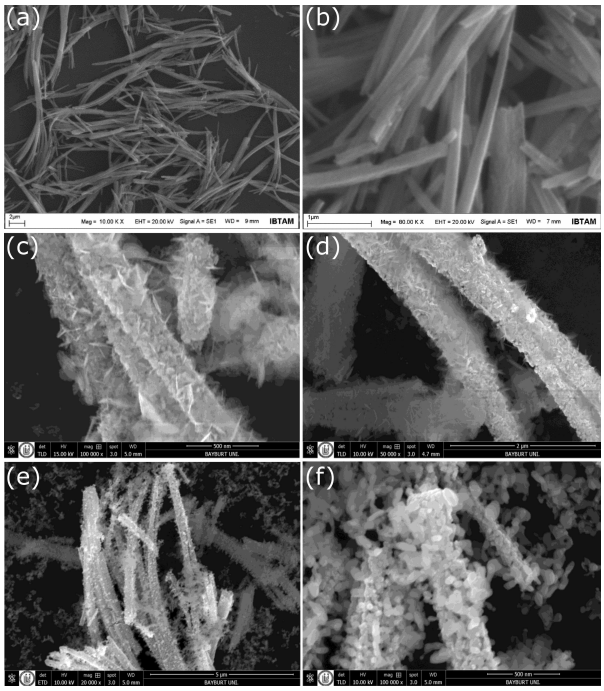

Fig. 4. SEM images of (a, b) SnO_2 NWs, (c, d) NiO/SnO_2 NWs calcined at 360 °C, (e, f) NiO/SnO_2 NWs calcined at 650 °C.

In the nanowires produced using PEG, only the peaks of the (−111), (200), (002), (111), (021), (−221), (−223), (221), and (−131) planes of the $Sn(COO)_2$ structure were observed before the heat treatment. It was also found that the heat-treated sample at 500 °C is in the tetragonal rutile SnO_2 phase given by PDF # 41-1445 card number. The observed diffraction patterns at 26.5°, 33.8°, 37.8°, 51.7°, 54.7°, 57.9°, 61.7°, 64.7°, 65.8°, 71.3°, and 79.3° correspond to the planes of (110), (101), (200), (211), (220), (002), (310), (112), (301), (202), and (321), respectively. In the XRD analysis of the material formed by precipitation of Ni^{2+} ions by NH_4OH on SnO_2 nanowires, in addition to the peaks of SnO_2, peaks corresponding to the planes (001), (100), (101), (110), (201) were observed at the angle values of 19.25°, 33.06°, 38.54°, 59.05°, and 72.7°, respectively. It was seen that this result matches with the $Ni(OH)_2$ structure given by the PDF#14-0117 card number. In the material heat treated at 360 °C and 650 °C, besides the peaks of SnO_2, peaks belonging to planes (111), (200), (220), and (311) were observed at angles of 37.24°, 43.27°, 62.87°, and 75.41°, which are thought to belong to NiO. The structure matches with the face-centred cubic NiO phase given by the card number PDF # 47-1049.

Park et al. [45] have shown that the NiO phase forms at temperatures higher than 300 °C. This result has a very good agreement with the present study. The material containing NiO/SnO_2 nanowires heat-treated at 650 °C exhibited sharper diffraction peaks than the heat-treated sample at 360 °C. According to this, the crystallinity of the heat-treated hybrid material at 650 °C is better.

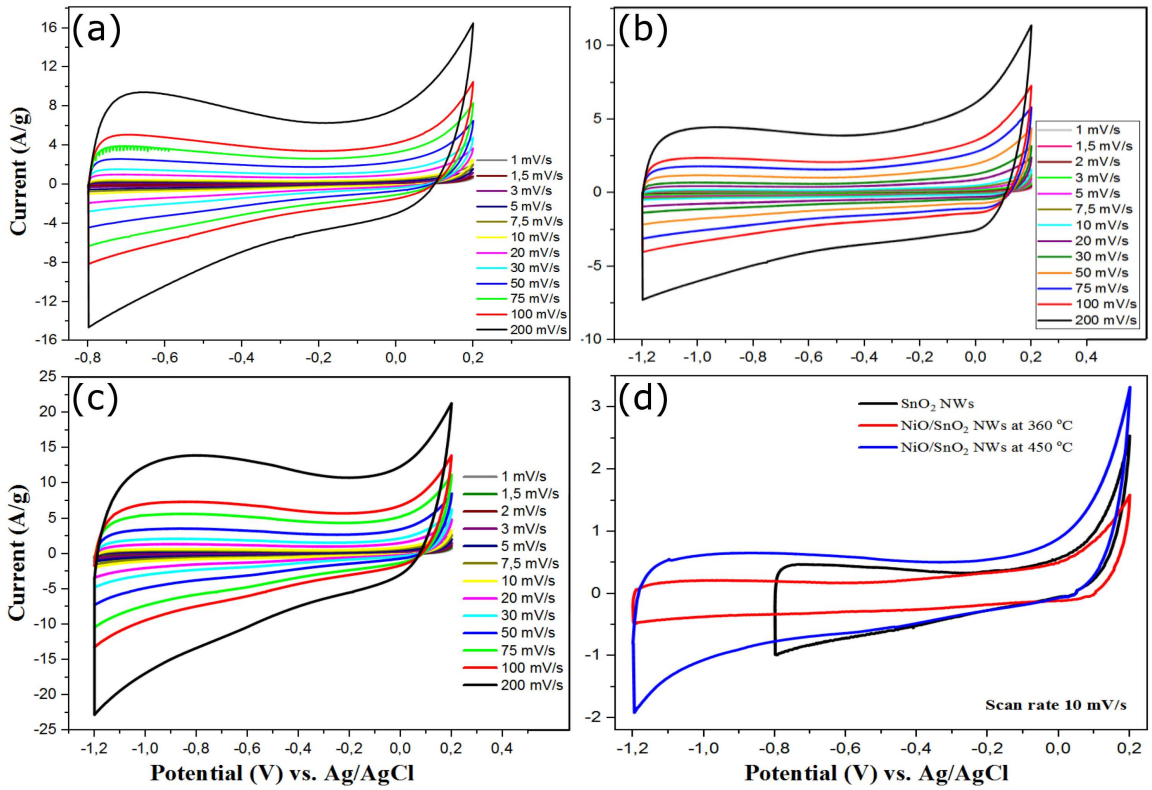

Fig. 5. CV curves of (a) SnO_2 NWs, (b) NiO/SnO_2 NWs calcined at 360 °C, (c) NiO/SnO_2 NWs calcined at 450 °C, (d) comparison of CV curves at a scan rate of 10 mV/s.

Figure 4 shows the SEM images of the SnO_2 and NiO/SnO_2 nanowires at different magnifications. It can be seen that the SnO_2 nanowires, heat treated at 500 °C, have diameters ranging from 100 to 250 nm and also vary in size from 6 to 10 μm (Fig. 4a and b). Figure 4c and d shows SEM images of NiO/SnO_2 hybrid nanowires heat-treated at 360 °C. The presence of NiO leafy structures on SnO_2 nanowires can be seen. The NiO leafy structure grew homogeneously throughout the nanowires. The H3 hysteresis observed in the N_2 adsorption-desorption isotherm curves, originates from the NiO leafy structure.

Also, the leafy shape NiO structures on the nanowires are the reason for the increase in the BET surface area. The NiO leafy structure on SnO_2 nanowires has changed to a more spherical structure (Fig. 4e and f) as a result of increase of the heat treatment temperature to 650 °C. The transformation of the NiO leaf structure into a spherical shape explains the decrease in the BET surface area. Cyclic voltammetry (CV) is one of the important methods used in the investigation of electrochemical properties. The electrochemical performance of electrodes containing SnO_2 and NiO/SnO_2 nanowires was investigated using a three-electrode cell in 6 M KOH. In particular, electrodes containing NiO/SnO_2 nanowires showed a rectangular shape similar to the CV curve of the ideal supercapacitor (Fig. 5). As the heat treatment temperature increased, a noticeable increase was observed in the area under the curve. It can be seen that the working potential window of the SnO_2 electrode, in the range of -0.8 V to 0.2 V, is extended to the range of -1.2 V to 0.2 V by the addition of NiO to the structure (Fig. 5d).

Typically, specific capacitance (C) is used to characterize the performance of electrode material. Figure 6 shows the specific capacitance changes calculated from the long-term charge-discharge curves for the different electrodes. The specific capacitance is also evaluated according to the following equation [43]:

$$C = \frac{I\Delta t}{m\Delta V}, \tag{1}$$

where I is the discharge current, Δt is the discharge time, ΔV is the potential window, and m is the mass of nanowires. All of the electrodes were charged-discharged for at least 3000 cycles at 1 A/g. The specific capacitance of the electrode containing only SnO_2 nanowires was approximately 60 F/g and no significant loss of capacitance was observed with long-term charge-discharge measurements. Among the electrodes containing NiO/SnO_2 nanowires, the best electrochemical performance was shown by the electrode heat treated at 450 °C. The initially observed specific capacitance was $\approx$ 143 F/g. After 400 continuous charge-discharge cycles the specific capacitance decreased to 130 F/g and continued to charge-discharge stably for 3000 cycles.

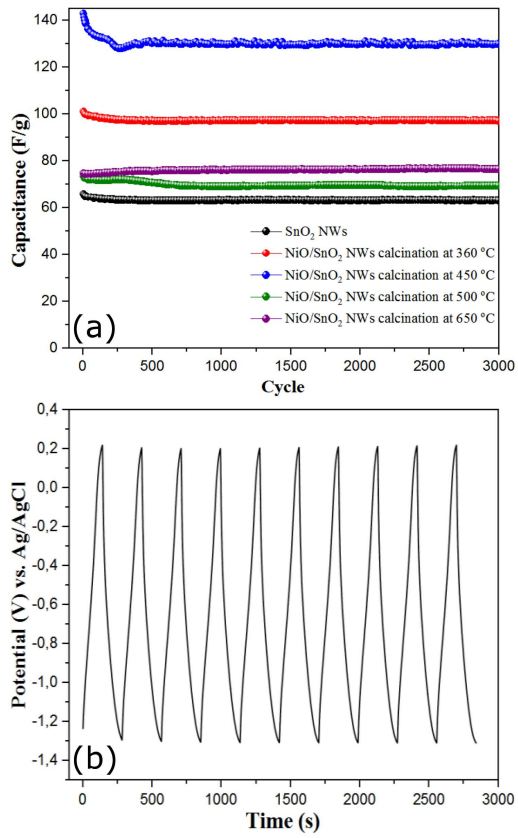

Fig. 6. (a) Variation of capacitance as a function of cycle number of SnO_2 and NiO/SnO_2 NWs at different calcination temperature. (b) The first ten cyclic charge-discharge curves of NiO/SnO_2 NWs calcination at 450 °C.

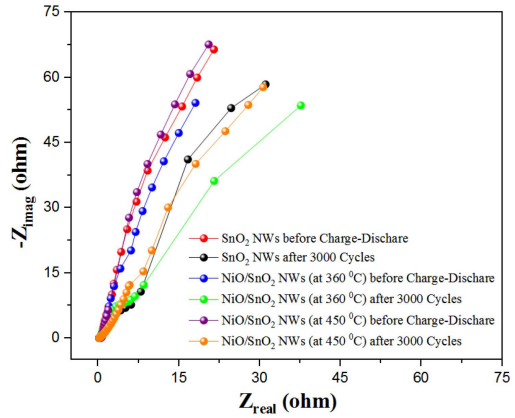

Fig. 7. Nyquist plots of SnO_2 and NiO/SnO_2 NWs at different calcination temperature at open circuit potential.

Figure 7 shows the Nyquist curves that were taken immediately after the CV measurements and after 3000 continuous charge-discharge cycles. The slope of the linear curve in the middle frequency region, for all electrodes, is greater than 45°, which is a good indicator for the generated supercapacitor electrodes. In general, the decrease in electrode performance after prolonged charge-discharge cycles is manifested by a decrease in the theta (θ) value. This diminution amount is a minimum for the NiO/SnO_2 NW electrode, especially obtained at 450 °C, with a decrease from 75° to 67° being observed.

4. Conclusions

In this study, SnO_2 material was produced in nanowire form in a very short time and by an inexpensive method which takes advantage of PEG's one-way chain growth. It was also found that the electrodes with NiO/SnO_2 structure are very important in terms of energy density since they have a much wider operating potential range than SnO_2 electrodes, and many electrodes in the literature. Electrochemical tests also showed that the NiO/SnO_2 electrode, heat-treated at 450 °C, has the best performance. This is thought to result from the leafy NiO structures on the SnO_2 nanowire surface.

Acknowledgments

This work was supported by Inonu University with the project numbers I.U.FLY-2018-1268 and I.U.2015/67.

References

[1] M.A.A.M. Abdah, N.H.N. Azman, S. Kulandaivalu, Y. Sulaiman, *Mater. Des.* **186**, 108199 (2019).

[2] X. Shi, S. Zheng, Z.S. Wu, X. Bao, *J. Energy Chem.* **27**, 25 (2018).

[3] Z.S. Iro, C. Subramani, S.S. Dash, *Int. J. Electrochem. Sci.* **11**, 10628 (2016).

[4] K. Wu, J. Zhao, X. Zhang, H. Zhou, M. Wu, *J. Taiwan Instit. Chem. Eng.* **102**, 212 (2019).

[5] W. Wu, D. Niu, J. Zhu, et al., *Ceram. Int.* **45**, 16261 (2019).

[6] R. Atchudan, T.N.J.I. Edison, S. Perumal, P. Thirukumaran, R. Vinodh, Y.R. Lee, *J. Taiwan Instit. Chem. Eng.* **102**, 475 (2019).

[7] A. Afif, S.M.H. Rahman, A.T. Azad, J. Zaini, M.A. Islan, A.K. Azad, *J. Energy Storage* **25**, 100852 (2019).

[8] A. Queraltó, A. Pérezdel Pino, C. Logofatu, A. Datcu, R. Amade, E. Bertran-Serra, E. György, *Ceram. Int.* **44**, 20409 (2018).

[9] P. Pascariu, A. Airinei, N. Olaru, I. Petrila, V. Nica, L. Sacarescu, F. Tudorache, *Sens. Actuat. B* **222**, 1024 (2016).

[10] J. Zhang, Y. Sun, J. Xu, *Micro Nano Lett.* **14**, 254 (2019).

[11] Y.R. Ahn, M.Y. Song, S.M. Jo, C.R. Park, D.Y. Kim, *Nanotechnology* **17**, 2865 (2006).

[12] C.C. Hu, Y.H. Huang, K.H. Chang, *J. Power Sourc.* **108**, 117 (2002).

[13] F.E. Atalay, D. Asma, H. Kaya, E. Ozbey, *Mater. Sci. Semicond. Process.* **38**, 314 (2015).

[14] J. Yan, T. Wei, J. Cheng, Z. Fan, M. Zhang, *Mater. Res. Bull.* **45**, 210 (2010).

[15] J. Jiang, A. Kucernak, *Electrochim. Acta* **47**, 2381 (2002).

[16] V.D. Patake, C.D. Lokhande, O.S. Joo, *Appl. Surf. Sci.* **255**, 4192 (2009).

[17] F.E. Atalay, H. Kaya, D. Asma, A. Bingöl, *Biointerface Res. Appl. Chem.* **6**, 1099 (2016).

[18] S.G. Kandalkar, J.L. Gunjakar, C.D. Lokhande, *Appl. Surf. Sci.* **254**, 5540 (2008).

[19] U.M. Patil, R.R. Salunkhe, K.V. Gurav, C.D. Lokhande, *Appl. Surf. Sci.* **255**, 2603 (2008).

[20] P.A. Nelson, J.R. Owen, *J. Electrochem. Soc.* **150**, A1313 (2003).

[21] N. Miura, S. Oonishi, K.R. Prasad, *Electrochem. Solid State Lett.* **7**, A247 (2004).

[22] C.C. Hu, C.M. Huang, K.H. Chang, *J. Power Sources* **185**, 1594 (2008).

[23] M. Nakayama, A. Tanaka, Y. Sato, T. Tonosaki, K. Ogura, *Langmuir* **21**, 5907 (2005).

[24] D.L. da Silva, R.G. Delatorre, G. Pattanaik, G. Zangari, W. Figueiredo, R.-P. Blum, H. Niehus, A.A. Pasal, *J. Electrochem. Soc.* **155**, E14 (2008).

[25] X. Zhou, H. Chen, D. Shu, C. He, J. Nan, *J. Phys. Chem. Solids* **70**, 495 (2009).

[26] B. Babakhani, D.G. Ivey, *J. Power Sourc.* **195**, 2110 (2010).

[27] D. Dodoo-Arhina, R.A. Nuamaha, P.K. Jainb, D.O. Obada, A. Yaya, *Results Phys.* **9**, 1391 (2018).

[28] S. Das, V. Jayaraman, *Progr. Mater. Sci.* **66**, 112 (2014).

[29] J. Liu, Y. Li, X. Huang, R. Ding, Y. Hu, J. Jiang, L. Liao, *J. Mater. Chem.* **19**, 1859 (2009).

[30] J.H. Shin, H.M. Park, J.Y. Song, *J. Alloys Comp.* **551**, 451 (2013).

[31] H.J. Snaith, C. Ducati, *Nano Lett.* **10**, 1259 (2010).

[32] H.W. Song, N. Li, H. Cui, C.X. Wang, *J. Mater. Chem. A* **1**, 7558 (2013).

[33] R.B. Rakhi, W. Chen, D. Cha, H.N. Alshareef, *J. Mater. Chem.* **21**, 16197 (2011).

[34] A.A. Firooz, A.R. Mahjoub, A.A. Khodadadi, *Sens. Actuat. B* **141**, 89 (2009).

[35] G.F. Xia, N. Li, D.Y. Li, R.Q. Liu, N. Xiao, D. Tian, *Mater. Lett.* **65**, 3377 (2011).

[36] Y. Chen, Q.Z. Huang, J. Wang, Q. Wang, J.M. Xue, *J. Mater. Chem.* **21**, 17448 (2011).

[37] F. Pourfayaz, A. Khodadadi, Y. Mortazavi, S.S. Mohajerzadeh, *Sens. Actuat. B* **108**, 172 (2005).

[38] H. Cui, Y. Liu, W. Ren, M. Wang, Y. Zhao, *Nanotechnology* **24**, 345602 (2013).

[39] Y.X. Yin, L.Y. Jiang, L.J. Wan, C.J. Li, Y.G. Guo, *Nanoscale* **3**, 1802 (2011).

[40] M. Zhao, Q. Zhao, J. Qiu, H. Xuea, H. Pang, *RSC Adv.* **6**, 95449 (2016).

[41] S. Ren, Y. Yang, M. Xu, H. Cai, C. Hao, X. Wang, *Coll. Surf. A* **444**, 26 (2014).

[42] S.K. Kwon, D.H. Kim, *J. Korean Phys. Soc.* **49**, 1421 (2006).

[43] F.E. Atalay, D. Asma, H. Kaya, A. Bingol, P. Yaya, *Nanomater. Nanotechnol.* **6**, 1 (2016).

[44] K.S.W. Sing, D.H. Everett, R.A.W. Haul, L. Moscou, R.A. Pierotti, J. Rouquerol, T. Siemieniewska, *Pure Appl. Chem.* **57**, 603 (1985).

[45] J.Y. Park, S.W. Choi, S.H. Jung, S.S. Kim, *J. Nanosci. Nanotechnol.* **12**, 1288 (2012).